Emulsifier peptides derived from seaweed, methanotrophic bacteria, and potato proteins identified by quantitative proteomics and bioinformatics

Betül Yesiltas [a,*,1], Simon Gregersen [b,*,1], Linea Lægsgaard [a], Maja L. Brinch [a], Tobias H. Olsen [d], Paolo Marcatili [d], Michael T. Overgaard [b], Egon B. Hansen [a], Charlotte Jacobsen [a], Pedro J. García-Moreno [a,c,*]

[a] National Food Institute, Technical University of Denmark, Denmark
[b] Department of Chemistry and Bioscience, Aalborg University, Denmark
[c] Department of Chemical Engineering, University of Granada, Spain
[d] Department of Bio and Health Informatics, Technical University of Denmark, Denmark

ARTICLE INFO

ABSTRACT

Global focus on sustainability has accelerated research into alternative non-animal sources of food protein and functional food ingredients. Amphiphilic peptides represent a class of promising biomolecules to replace chemical emulsifiers in food emulsions. In contrast to traditional trial-and-error enzymatic hydrolysis, this study utilizes a bottom-up approach combining quantitative proteomics, bioinformatics prediction, and functional validation to identify novel emulsifier peptides from seaweed, methanotrophic bacteria, and potatoes. *In vitro* functional validation reveal that all protein sources contained embedded novel emulsifier peptides comparable to or better than sodium caseinate (CAS). Thus, peptides efficiently reduced oil–water interfacial tension and generated physically stable emulsions with higher net zeta potential and smaller droplet sizes than CAS. *In silico* structure modelling provided further insight on peptide structure and the link to emulsifying potential. This study clearly demonstrates the potential and broad applicability of the bottom-up approach for identification of abundant and potent emulsifier peptides.

1. Introduction

Due to growing consumer demand for clean label and sustainable food ingredients (Asioli et al., 2017), the search for potent, natural replacements for chemical additives (e.g. emulsifiers), is rapidly developing. In light of the tremendous carbon footprint imposed by the food sector (Poore & Nemecek, 2019), utilization of alternative sources and protein-rich industrial side-streams, as well as zero-waste ambitions, has attracted immense attention. As proteins may furthermore be processed to release functional and bioactive peptides (Hajfathalian, Ghelichi, García-Moreno, Moltke Sørensen, & Jacobsen, 2018), they may be regarded as a potential vast resource of natural ingredients to both replace chemical additives while also improving nutritional quality and sustainability. Consequently, peptides from various sources of relevance in foods (e.g. dairy, plant, animal, and seafood) have been reported to display diverse functional properties (Ashaolu, 2020; Hajfathalian et al., 2018; Jafarpour et al., 2020). One specific class, amphiphilic peptides, has received tremendous interest, due to the diverse functional aspects related to this physicochemical property. Amphiphilicity is a crucial factor in peptide self-assembly and therefore also of tremendous importance in the interfacial properties of peptides (Cui et al., 2010). In foods, interfacial properties are important for functionalities such as emulsification (García-Moreno, Jacobsen et al., 2020) and foaming (Jafarpour et al., 2020). Fish oil-in-water emulsions are attractive as delivery systems in omega-3 PUFA-enriched foods (Jacobsen, 2015). Emulsion stability is closely related to the applied emulsifier(s), as they govern oil dispersion during production as well as physical stability during storage. Emulsifiers adsorb to the oil–water interface, forming a layer to protect emulsion droplets from aggregation (e.g., flocculation, coalescence) by providing steric hindrance and/or electrostatic repulsions (McClements, 2016). Interfacial properties also play a key role in peptide interaction with biological membranes and therefore also

relate to food preservation through antimicrobial activity (Findlay et al., 2010). In fact, these properties may coincide, when assessing the functional properties of amphiphilic peptides (Dexter & Middelberg, 2008; Enser et al., 1990). Interfacial properties of amphiphilic peptides and their adsorption characteristics at the oil–water interface are highly complex but ultimately governed by the primary structure and thus influenced by various factors such as length, charge, concentration, and particularly conformation (Cheng et al., 2010, 2014; Jafarpour, Gomes, Gregersen, Sloth, Jacobsen, et al., 2020; García-Moreno, Gregersen et al., 2020; García-Moreno, Jacobsen et al., 2020; Olsen et al., 2020). Peptides, which may also exhibit antioxidant activity, have furthermore been reported to show great potential for enhancing oxidative stability in oil-in-water emulsions (Cheng et al., 2010; García-Moreno, Gregersen et al., 2020; García-Moreno, Jacobsen et al., 2020).

Traditionally, identification of new peptide emulsifiers from relevant food protein sources has been accomplished through a top-down approach, where a protein biomass is subjected to enzymatic hydrolysis to various degrees in a trial-and-error approach (Cheng et al., 2010; Hajfathalian et al., 2018). Emulsifier peptides may subsequently be identified through different steps of bulk functional validation, hydrolysate fractionation, and finally and very rarely peptide identification by e.g. mass spectrometry (Falade et al., 2021; Hajfathalian et al., 2018; Wu et al., 2018). Peptides with α-helix or β-strand secondary structures show facial amphiphilicity and locate themselves parallel to the oil–water interface by projecting lipophilic parts to the non-polar phase and hydrophilic parts to the polar phase (Dexter & Middelberg, 2008). Some peptides may however exhibit axial amphiphilicity by orienting their hydrophilic and lipophilic parts perpendicular to the oil–water interface, independent of the secondary structure. Building on these physical prerequisites for peptide emulsification activity, we recently identified a range of emulsifier peptides embedded in potato proteins using a conceptually new bottom-up approach, which combines quantitative proteomics and bioinformatic prediction to identify potent emulsifier peptides releasable from abundant proteins in a given biomass (García-Moreno, Gregersen et al., 2020; García-Moreno, Jacobsen et al., 2020). The bottom-up approach fundamentally differs from the traditional top-down approach for bioactive peptide discovery, thereby removing the need for subsequent, labor-intensive fractionation and work-up to identify potential bioactive peptides. Application of bioinformatic prediction for *in silico* identification of new food bioactive peptides based on either physical model computation or artificial intelligence (e.g. machine learning and neural networks) is rapidly developing (García-Moreno, Gregersen et al., 2020; García-Moreno, Jacobsen et al., 2020; Minkiewicz et al., 2019; Olsen et al., 2020; Xu et al., 2018). The studies by García-Moreno et al. (García-Moreno, Gregersen et al., 2020; García-Moreno, Jacobsen et al., 2020) indicated that even though the computed amphiphilic scores did not fully correlate with their structure and emulsifying activity, it was overall a good prediction of peptide emulsification potential. A similar approach has been applied on e.g. hydrolysates from industrial codfish waste-streams, where bioinformatic prediction was combined with proteomics studies in order to identify specific bioactive peptides responsible for the bulk emulsifying properties (Jafarpour et al., 2020).

In this work, we applied the recently proposed bottom-up approach (García-Moreno, Gregersen et al., 2020) to identify new emulsifier peptides embedded in high abundance proteins of new, potential protein sources for use in foods. To illustrate the broad applicability of the approach and its potential for protein valorization, we selected two highly different protein sources, both adhering to the overall goal of sustainability. On one hand, we included a biomass from the fermentation of methanotrophic bacteria (*M. capsulatus* and *Ralstonia* sp.) currently employed for animal feed, and on the other hand, a side stream from industrial seaweed (*E. denticulatum*) processing and carrageenan production. Additionally, a set of peptides derived from previously verified peptide emulsifiers from potato (*S. tuberosum*) were included. These peptides were included as they were experimentally identified by

LC-MS/MS and originated from the highly abundant storage protein patatin (García-Moreno, Gregersen et al., 2020). Moreover, additional data will prove useful in understanding the structure/function relationship of emulsifier peptides. Thus, this study initially (i) characterized the methanotrophic biomass using quantitative bottom-up proteomics (BUP), and subsequently (ii) predicted potential peptide emulsifiers, with different secondary structure (α-helix, β-sheet and unordered), embedded in the most abundant proteins from a seaweed extract and a bacterial biomass using bioinformatic prediction. Moreover, (iii) emulsifying activity of the predicted peptides was validated *in vitro* by their effect on the oil–water interfacial tension and the physical stability of 5% fish oil-in-water emulsions during six days of storage mimicking delivery emulsions for omega-3 fatty acids. Next, (iv) multivariate data analysis (principal component analysis) was used to evaluate the importance of different physicochemical properties on peptide functionality and for selection of the most promising lead peptides. Lastly, (v) templated homology modelling was used to investigate putative interfacial structure and explain emulsifying properties of the selected peptides.

2. Materials and methods

2.1. Materials

Synthetic peptides (purity > 70% by HPLC) were purchased (China Peptides Co., Ltd, Shanghai, China). Sodium caseinate (Miprodan 30) with 93.5% protein (Nx6.38, dry matter) was provided by Arla Foods Ingredients amba (Viby J, Denmark) and used as a positive control for emulsifying activity. Cod liver oil was provided by Vesteraalens (Sortland, Norway) and stored in brown bottles at –40 °C until use. Medium chain triglycerides (MCT) oil (WITARIX MCT 60/40) was purchased from IOI Oleo GmbH (Hamburg, Germany). Protein raw materials used in this study originated from seaweed (*E. denticulatum*), a fermented biomass of methanotrophic bacteria and potato (*S. tuberosum*). Microbial protein was delivered by Unibio (Kalundborg, Denmark) as a homogenized, protein-rich biomass of methane metabolizing bacteria (primarily *M. capsulatus* (90%) and *Ralstonia* sp. (formerly known as *A. acidovorans*) (8%)), fermented using Unibio's proprietary U-Loop® reactor technology (Larsen, 2002). Seaweed and potato proteins described in this study were delivered by CP Kelco (Lille Skensved, Denmark) and KMC AmbA (Brande, Denmark), respectively, as previously reported (García-Moreno et al., 2020; Gregersen et al., 2020). The rest of reagents used were of analytical grade.

2.2. Methods

2.2.1. Proteomics analysis of microbial proteins by 1D SDS-PAGE and LC-MS/MS

Microbial protein was analyzed as previously described (García-Moreno, Gregersen et al., 2020). The homogenized biomass was solubilized to a target protein concentration of 2 mg/mL in 200 mM ammonium bicarbonate (ABC) with 2% SDS (pH 9.5) and insolubles were sedimented by centrifugation. Aliquots of 20 µg protein were analyzed by SDS-PAGE using precast 4–20% gradient gels (GenScript, Piscataway, NJ, USA) under reducing conditions and in accordance with manufacturer guidelines. As molecular weight marker, Pierce Unstained Protein MW Marker (ThermoFischer Scientific, Waltham, MA, USA) was used. Proteins were stained using Coomassie Brilliant Blue G250 (Sigma, Darmstadt, Germany) and visualized using a ChemDoc MP Imaging System (Bio-Rad, Hercules, CA, USA).

Sample lanes were excised and divided into 6 fractions using the MW marker as guide fractions were in-gel digested as previously described using sequencing grade modified trypsin (Promega, Maddison, WI, USA). Following extraction, peptides were desalted using StageTips, Tryptic digests were analyzed by LC-ESI-MS/MS, consisting of an EASY-nLC system (Thermo Scientific, Bremen, Germany) on-line coupled to a

Q Exactive mass spectrometer via a Nanospray Flex ion source (Thermo Scientific). Peptides were loaded on an Acclaim Pepmap Nanotrap column (C18, 100 Å, 100 μm, 2 cm (Dionex, Sunnyvale, CA, USA)) followed by separation on an Acclaim Pepmap RSLC analytical column (C18, 100 Å, 75 μm, 50 cm (Dionex). Chromatography and data acquisition was performed as previously reported (García-Moreno, Gregersen et al., 2020).

2.2.2. Analysis of LC-MS/MS data by MaxQuant

The microbial biomass primarily constitutes of *M. capsulatus* and *Ralstonia* sp. with the relative abundances of 90% and 8%, respectively (Unibio supplied information). Consequently, the UniProt (UniProt Consortium, 2019) proteome for *M. capsulatus* (strain ATCC 33,009/NCIMB 11,132/Bath) (UP000006821) and *Ralstonia* sp. 25mfcol4.1 (NCBI:txid1761899) (UP000199332) were downloaded and both included as protein databases. LC-MS/MS data was analyzed in Max-Quant 1.6.0.16 (Cox & Mann, 2008; Tyanova et al., 2016), as previously described (García-Moreno, Gregersen et al., 2020). Briefly, protein identification was performed using a 1% FDR on both protein and peptide level, reverse sequences were used as decoys for FDR control, common contaminants were included, and quantification was done using both unique and razor peptides. Matching between runs and dependent peptides options were enabled. Protein quantification was performed using iBAQ (Schwanhäusser et al., 2011) and relative protein abundance was determined by relative iBAQ (riBAQ) (Shin et al., 2013). MaxQuant output files (txt folder) along with raw LC-MS/MS data are available through the linked Mendeley Data Repository (Gregersen, 2021).

2.2.3. Protein selection and bioinformatics prediction of embedded emulsifying peptides

Based on quantitative proteomics studies of microbial protein, highly abundant proteins (>1% relative abundance by riBAQ) were selected for bioinformatic analysis. Similarly, highly abundant proteins from an industrially relevant extract of *E. denticulatum* (Gregersen et al., 2020) were selected for computational analysis. Finally, four peptides, previously identified experimentally in tryptic hydrolysates from highly abundant potato proteins, were included (García-Moreno, Gregersen et al., 2020).

Full-length sequences from abundant microbial and seaweed proteins were analyzed using EmulsiPred (https://github.com/Marcat iliLab/EmulsiPred) (García-Moreno, Gregersen et al., 2020; García-Moreno, Jacobsen et al., 2020). Emulsifier peptides were identified based on their amphiphilicity in a given conformation at the oil–water interface: i) α-helix, ii) β-strand or iii) partly hydrophobic and partly hydrophilic with no specified secondary structure (γ-peptides). Experimental sequence coverage was determined using multiple sequence alignment in CLC Sequence Viewer 8.0 (https://www.qiagenbioinforma tics.com/).

2.2.4. Reduction of interfacial tension (IFT) by the selected peptides

The dynamic IFT of peptides at the oil–water interface was determined using an automated drop tensiometer OCA25 (DataPhysics Instruments GmbH, Filderstadt, Germany) at 25 °C. For the oil–water IFT measurement, a small drop of the peptide/sodium caseinate solutions (0.2 wt% in 10 mM sodium acetate-imidazole buffer, pH 7), buffer or MQ water solution was generated using the automated syringe into a quartz glass cuvette filled with MCT oil (WITARIX® MCT 60/40, IOI Oleo GmbH, Hamburg, Germany). The image of the pendant drop was recorded every 10 s over a period of 30 min and the drop shape was analyzed using the Young-Laplace equation as described in Yesiltas et al. (2019). Changes in the IFT (mN/m) were plotted as a function of time (min). All measurements were performed in duplicate.

2.2.5. Emulsion production and storage experiment

Fish oil-in-water emulsions were produced using 0.2 wt% peptide or

sodium caseinate as emulsifier. 0.2 wt% peptide/sodium caseinate was solubilized in 10 mM sodium acetate–imidazole buffer (pH 7) while shaken in a water bath (50 °C, 2 h) and hydrated overnight (100 rpm) at room temperature. Next day, 5 wt% fish oil was added into the aqueous phase and emulsified first with a handheld ultraturrax (Polytron, PT1200E, 18000 rpm, 30 s). After pre-homogenization, sonication (Microson XL2000, probe *P*1) was used as a secondary homogenization at 75% amplitude (max. amplitude 180 μm) for 30 s in two passes with 1 min break. Emulsions were produced in triplicate and pH was measured before and after emulsification. Emulsions were stored for six days at room temperature in darkness.

2.2.6. Physical stability of the emulsions

2.2.6.1. Creaming and oil rich phase accumulation on top.
When a cream layer was observed at the top and a clear water phase appeared at the bottom of the emulsion containing tube, creaming index (CI) was calculated as:

$$\mathrm{CI}(\%) = \frac{hW}{hT} \times 100$$

where h_W is the height of the clear water phase at the bottom and h_T is the total height of the 'emulsion'. Oil rich phase accumulation on top is similar to creaming but with an unclear phase at the bottom instead. Index for oil rich phase accumulation on top (OI) was calculated as follows;

$$\mathrm{OI}(\%) = \frac{hT - hW}{hT} \times 100$$

where h_T is the total height of the total emulsion and h_W is the height of the less opaque phase at the bottom.

CI and OI were determined by adding 2 mL emulsion to a 4 mL measuring cylinder and observations were recorded on days 0, 1 and 6 during storage.

2.2.6.2. Droplet size distribution.
Droplet size distribution was measured by laser diffraction in a Mastersizer 2000 (Malvern Instruments, Ltd., Worcestershire, UK). The emulsion was diluted in recirculating water (3000 rpm), until it reached an obscuration of 10–12%. The refractive indices of sunflower oil (1.469) and water (1.330) were used as particle and dispersant, respectively. Results are given in volume mean (D[4,3]) and surface area mean (D[3,2]) diameters. Measurements were performed in triplicate on days 0, 1, 3, and 6.

2.2.6.3. Zeta potential.
The zeta potential was measured in a Zetasizer Nano ZS (Malvern instruments Ltd., Worcestershire, UK) with a DTS1070 cell at 20 °C to identify the surface charge of the oil droplets, which are covered with peptides. Before analysis, the emulsion was diluted in buffer (20 μL emulsion in 10 mL buffer). The zeta potential range was set to −100 to + 50 mV. Measurements were performed in triplicate on day 1.

2.2.7. Protein modelling and peptide visualization

For the nine best performing emulsifier peptides, protein modelling was performed as previously described (García-Moreno, Gregersen et al., 2020) using the Swiss-Model Workspace (Waterhouse et al., 2018). *E. denticulatum* protein c7052_g1_i1.p1 (80-S-A, 83-S-B, and 86-S-B) was modelled using 26 kDa periplasmic immunogenic protein from *Brucella abortus* (STML ID 4hvz.1.M) as template. *E. denticulatum* protein c4354_g1_i1.p1 (82-S-A) was modelled using proximal thread matrix protein 1 (PTMP1) from *Mussel byssus* (STML ID 4cn9.2.A) as template. *E. denticulatum* protein c6313_g1_i1.p1 was modelled using GEBA250068378 from *Sulfurospirillum deleyianum* (STML ID 3nkg.1.A) as template. *M. capsulatus* protein G1UBD1 (Particulate methane monooxygenase alpha subunit) was modelled using its own crystal structure

(STML ID 3rgb.1.A). *M. capsulatus* protein Q60B76 (Putative lipoprotein) was modelled using lambda repressor (1–45) from the λ bacteriophage (STML ID 3woa.1) as template. *S. tuberosum* proteins Q3YJT3 and Q3YJT4 (Patatin-2-Kuras 1 and Patatin-1-Kuras 2) were both modelled using Patatin-17 from *S. tuberosum* (STML ID 4pka.1.A) as template. Models were subsequently visualized using The PyMOL Molecular Graphics System version 1.5.0 (Schrödinger, LLC.). Peptide visualization, including visible side chains, was done by applying the Swiss-Model hydrophobicity color scheme. Final figures were assembled and annotated in Inkscape version 0.92.3 (Inkscape project).

2.2.8. Statistical analysis

Statgraphics 18 (Statistical Graphics Corp., Rockville, MD, USA) was used for statistical analysis. Mean value and standard deviations were used for the data analysis. Multiple sample comparison was performed to identify the significant differences between samples and sampling days during storage. Mean values were compared using the Bonferroni test at $p < 0.05$ significance level. Principle component analysis (PCA) was also carried out using Statgraphics 18. Peptide codes are the objects and length, molecular weight (MW), amphiphilic score (AS), droplet size mean diameters (D[3,2] and D[4,3]) at day 0, interfacial tension (IFT), zeta potential, and isoelectric point (pI) are the selected measured variables. This analysis only includes the peptides that had values for each variable. Zeta potential values were included in their absolute values disregarding their charge to emphasize the magnitude of the charge potential. The PCA was carried out on the correlation matrix, standardizing each variable by subtracting the mean value and dividing by the standard deviation.

3. Results and discussion

3.1. Proteomics analysis of biomass from methane-based fermentation

Bottom-up shotgun proteomics analysis of the homogenized biomass resulted in identification of 1839 unique peptides distributed between 597 protein groups accounting for a total of 626 potential proteins (Table S1). This corresponds well with the level of protein complexity observed from SDS-PAGE analysis (Fig. S1). Applying SDS-PAGE and subsequent in-gel digestion not only provides visualization of the biomass proteome, but also facilitate pre-fractionation according to size, thereby allowing further depth in the proteomics analysis of the biomass. As expected, the majority of identified protein groups originated from *M. capsulatus* (549) accounting for 93.5% of the total sample protein (by riBAQ), while *Ralstonia* sp. specific or indistinguishable/conserved proteins accounted for a much lower content of the protein biomass (1.4% and 5.1%, respectively). This is in good agreement with the biomass supposedly consisting of 90% *M. capsulatus* and 8% *Ralstonia* sp. (Unibio supplied information).

On the single protein level, 16 protein groups were identified to each constitute >1% of the relative protein content. Hereof, 15 were unique proteins from *M. capsulatus* while one protein group contained a conserved protein between the two species (Table S2). Not surprisingly, a large proportion of the abundant proteins in the methanotrophic biomass are related to the methane metabolism (mca00680) KEGG pathway (Kanehisa & Goto, 2000).

3.2. Prediction of emulsifier peptides by bioinformatics

Abundant microbial proteins (Table S2) were selected for bioinformatics prediction of embedded emulsifier peptides. Similarly, abundant proteins from a recent study on hot-water extracts from the seaweed *E. denticulatum* (Gregersen et al., 2020) were included in the prediction. This was done to obtain a wide variety of peptides with potential emulsification activity and sufficient production yield. Lastly, four peptides, originating from the highly abundant potato (*S. tuberosum)* storage protein Patatin were included in the study. These peptides were

previously experimentally identified by LC-MS/MS following tryptic digestion and are derived from known emulsifier peptides (García-Moreno, Gregersen et al., 2020). In total, 28 potential emulsifier peptides (12 seaweed, 12 microbial and 4 potato peptides) with different predicted emulsification mechanism, were synthesized by a commercial peptide supplier (Table 1). The peptides varied in their physicochemical characteristics such as potential structure at the interface, length, net charge (pH 7), isoelectric point, and amphiphilicity.

Interestingly, the majority of predicted emulsifier peptides from the microbial biomass originate from either enzyme involved in methane metabolism or GroEL chaperonin 2. As these proteins are either membrane associated (Myronova et al., 2006) or form highly complex membrane-like macrostructures (Braig et al., 1994), they are thus likely to include highly amphiphilic regions, which may in turn prove to be excellent sources of emulsifier peptides. The genome and proteome of *E. denticulatum* is poorly described in the literature. Nevertheless, the majority of predicted seaweed emulsifier peptides originate from proteins predicted to be extracellular (Gregersen et al., 2020).

3.3. Interfacial tension

The ability of surface active compounds to decrease the oil–water interfacial tension (IFT) in emulsions is of great importance, as this ability favors the formation of emulsified oil droplets (Matsumura & Matsumiya, 2012; McClements, 2016). Therefore, the emulsifier peptides were tested to investigate their role on decreasing the IFT between MCT oil and buffer as a function of time. Some peptide solutions were cloudy (Table 2), indicating that peptides were not totally soluble in buffer, which could affect their affinity to the interface or emulsifying activity, and therefore the IFT results (García-Moreno, Gregersen et al., 2020). Hydrophobic domains are a prerequisite for peptide amphiphilicity, but as seen here, this may impair solubility and consequently functionality and applicability. Therefore, further refinement of prediction algorithms for emulsifying potential may capitalize greatly by the incorporation of solubility factor, which could potentially address this issue.

Results are compared based on their final IFT value at 30 min, since at this time point most of peptides reached the equilibrium. In addition, the speed of reaching the equilibrium after the analysis started is addressed, since it indicates the adsorption rate of the peptides at oil-water interfacial layer. IFT values at 30 min between MCT oil and MQ water or sodium caseinate (CAS) were 25 and 11 mN/m, respectively, which was in line with previous studies (García-Moreno, Gregersen et al., 2020). MCT oil-buffer IFT showed a remarkable decrease from 24.5 to 15.4 mN/m indicating its effect on decreasing IFT. However, this was not observed on peptide solutions prepared in the same buffer. It is worth noting that the mechanism for the buffer to reduce IFT is different from the peptide solutions, since the reduction is not sharp immediately after time zero as observed for the peptides.

3.3.1. Seaweed-derived peptides

IFT of seaweed peptides ranged between 8.6 and 25.4 mN/m at 30 min (Fig. 1A). 89-S-G had as high IFT as MQ water, which indicates a very low surface activity. This is contradicting its high amphiphilic score as this peptide has the highest among all (Table 1). Similar to 89-S-G, other peptides with gamma conformation (91-S-G, 87-S-G, 90-S-G, and 88-S-G) were also not very efficient in lowering the MCT oil–water IFT (end values of >20 mN/m). García-Moreno, Gregersen et al. (2020) reported that the peptides with gamma conformation (potentially exhibiting perpendicular amphiphilicity) showed higher IFT when they were shorter than 18 AAs. Indeed, 90-S-G and 91-S-G confirmed their findings. However, 87-S-G, 88-S-G, and 89-S-G were not sufficiently surface-active to decrease the IFT in spite of their length with 30, 21, and 30 AAs, respectively. On the other hand, IFT values at 30 min for 83-S-B and 84-S-B were around 13.7 and 13.0 mN/m, respectively, indicating high surface-activity for these peptides as these values are close to the

Table 1

Amino acid sequence, length, molecular weight (MW), purity, net charge (z) at pH 7, isoelectric point (pI), amphiphilic score (score), protein of origin, and relative protein abundance (by riBAQ in the raw samples analyzed in this and previous studies) (García-Moreno et al., 2020; Gregersen et al., 2020) for the potential emulsifier peptides assayed in this study.

Peptide	Amino acid sequence	Length	MW (Da)	Purity (%)	z (pH7)*	pI*	Score	Protein AC	Abundance
80-S-A	IGYTVRNSLRVTVRDLSNLGLILDALVR	28	3128.08	73.65	2	10.84	3.30	c7052_g1_i1	33%/25%**
81-S-A	AVKDAVRRATLLTKAAGTGLGKVLS	25	2497.38	84.25	4	11.50	2.90	c7052_g1_i1	33%/25%**
82-S-A	IDSSFDSLPTDVVRVANSSCDAVE	24	2527.12	93.35	−4.1	3.18	3.28	c4354_g1_i1	4.0%/0.3%**
83-S-B	RAGSNSLSRISFGISNEADLRDQAR	25	2721.34	75.52	1	10.24	3.18	c7052_g1_i1	33%/25%**
84-S-B	VGFACSGSAQTYLSFEGDNTGRGEEEVAI	29	2995.19	79.58	−4.1	3.44	2.75	c6313_g1_i1	32%/23%**
85-S-B	LSIREGGRSTGGFSAQVRAR	20	2105.35	73.47	3	12.10	3.27	c7052_g1_i1	33%/25%**
86-S-B	ELQVSARVTLEIEL	14	1600.25	73.20	−2	3.85	5.43	c7052_g1_i1	33%/25%**
87-S-G	RELQRDDNVRNVRILLSSLVLLLDWLVCLL	30	3578.29	85.53	−0.1	6.28	5.72	c1505_g2_i1	17%/28%**
88-S-G	AVLVVCLQQVRELQRDDNVRN	21	2468.24	80.15	−0.1	6.26	5.06	c1505_g2_i1	17%/28%**
89-S-G	VVGAFALIVVILLGMWAVHNKSKNQSDSDY	30	3276.22	74.89	0.1	7.71	6.83	c8421_g1_i1	1.6%/0.0%**
90-S-G	VIVILTDGRESPRRADQ	17	1925.18	83.14	0	6.95	5.25	c4354_g1_i1	4.0%/0.3%**
91-S-G	DEGDDRIVVL	10	1120.22	89.43	−3	3.32	4.88	c8421_g1_i1	1.6%/0.0%**
92-U-A	LRTFGKDVAPVSAFFSAFMSILIYFMWHF	29	3430.11	79.66	1.1	9.74	2.45	Q607G3	8.9%
93-U-A	NYVRTGTPEYIRMVEK	16	1956.26	83.81	1	9.19	2.36	Q607G3	8.9%
94-U-A	DIKRGIDQAVGVVVEELKKLSKPCTD	26	2841.33	76.82	−0.1	6.38	4.68	Q607Q3	3.1%
95-U-A	KAIAQVGTISANSDESIGQIIAQAMDTVG	29	2889.24	79.96	−2	3.54	3.34	Q607Q3	3.1%
96-U-B	VRLEIGKTYDFRVVLKARRPGDWHVH	26	3149.07	85.20	3.2	10.74	4.16	G1UBD1	7.5%
97-U-B	KVKINETVEIKGKFHV	16	1869.24	85.94	2.1	10.24	5.07	G1UBD1	7.5%
98-U-B	FYGTLDGFIKARDTRTGELKWQFQLPSGV	29	3332.18	74.19	1	9.45	3.25	Q60AR6	7.3%
99-U-G	DWDFWSDWKDRRLWVTVTPIVLVTFPAAV	29	3520.06	76.27	−1	4.19	4.82	Q607G3	8.9%
100-U-G	RADELVSATDRKVAMGFLAATILIVVMA	28	2962.58	81.74	0	6.69	4.54	G1UBD1	7.5%
101-U-G	VVFFVIVGSYHIHAMLTMGDWDFWSDWKDR	30	3659.21	79.65	−1.8	5.04	4.11	Q607G3	8.9%
102-U-G	RKQIEDTTSDYDREKLQERVAKLAGGVAVI	30	3390.22	75.56	0	6.85	5.18	Q607Q3	3.1%
103-U-G	RSPQKKESDMMKATKFAVVLMAAGLTVGCA	30	3170.25	78.37	2.9	10.22	4.96	Q60B76	4.1%
104-P-G	GIIPATILEFLEGLQEVDNNKDAR	25	2784.12	77.57	−3	3.79	3.69	Q3YJT3***	2.5%/5.3%***
105-P-G	GIIPGTILEFLEGQLQK	17	1856.20	82.64	−1	4.15	2.45	Q3YJT4***	12%/4.2%***
106-P-A	SVSEDNHETYEVALKR	16	1877.00	73.62	−1.9	4.52	<2	Q3YJS9***	2.9%/5.8%***
107-P-A	DNPETYEEALKR	12	1464.56	92.64	−2	4.04	<2	Q2MY60***	13%/17%***

'S, U, and P' letters in the sample names encode seaweed, microbial, and potato, respectively; 'A, B, and G' letters encode alpha, beta, and gamma indicating potential secondary structure of peptides. *z at pH 7 and pI were calculated using peptide property calculator (Innovagen AB, Lund, Sweden). ** Protein abundance is listed for both the seaweed (*E. denticulatum*) extracts (A and B, respectively) analyzed in the study (Gregersen et al., 2020). ***Peptides were identified in numerous patatin isoforms (García-Moreno, Gregersen et al., 2020), but for simplicity, the most abundant isoform is listed, while the protein abundance is the cumulative, relative abundance of all proteins isoforms containing the peptide and hence reflects a potential yield. Calculations are based on the content in the high quality food-grade protein extract (KMC-Food) and the heat/acid precipitated feed-grade protein (KMC-Feed), respectively.

positive control, CAS (11.2 mN/m). CAS is an oil–water interface active milk protein with good emulsifying activity commonly used in food industry.

IFT for most of the peptides levelled off within the first few minutes and then stayed close to the same value (Fig. 1A). However, this trend was not observed for the following peptides: 82-S-A, 84-S-B, 85-S-B, 86-S-B, 87-S-G, and 91-S-G. For these peptides, equilibrium was not reached until 15–20 min and in the case of 85-S-B, 87-S-G, and 91-S-G, IFT kept decreasing at a constant rate throughout the 30 min. This indicated that longer time was required for adsorption and rearrangement of these peptides at the oil–water interface. Decreased adsorption kinetics has previously been linked with the increasing peptide length (82-S-A, 84-S-B and 87-S-G) due to lower diffusion rate. The observation may also be a result of poor peptide solubility for some peptides (86-S-B and 91-S-G). Nevertheless, 80-S-A and 86-S-B showed lower equilibrium IFT values compared to CAS. This is in line with previous results on potato peptides, where amphiphilic α-helix peptides above 18 AAs and amphiphilic β-peptides around 13–14 AAs reduced the IFT significantly (García-Moreno, Gregersen et al., 2020). Moreover, 86-S-B had one of the highest amphiphilic score (5.43) among all predicted peptide emulsifiers (Table 1). Interestingly, this peptide had a solubility issue resulting in a cloudy solution when dissolved in the buffer (Table 2), which could be due to its high amphiphilicity and therefore some extremely hydrophobic regions leading to peptide aggregation and/or self-assembly due to hydrophobic interactions. Formation of nanoassemblies and macromolecular self-assembly for amphiphilic peptides in aqueous solution has been widely reported (Cui et al., 2010) and have attracted attention as e.g. potential drug delivery systems (Feger et al., 2020). Nevertheless, this insolubility apparently did not fully impair reduction of oil–water IFT and may in addition be interesting to investigate further for other

applications than emulsification. It is worth noting that when solubility is an issue, undissolved peptides may accumulate at the bottom of the oil droplet weighing it down and causing shape deformation, which could result in low IFT results (e.g., even though it is not related to their surface properties).

3.3.2. Methanotrophic bacteria-derived peptides

IFT values at 30 min for microbial peptides varied between 11.0 and 20.6 mN/m (Fig. 1B), which is a smaller range compared to seaweed peptides (Fig. 1A). Peptides 101-U-G, 100-U-G, and 92-U-A had IFT values around 24 mN/m at the beginning of the analysis and decreased to 20.6, 17.8, and 16.9 mN/m, respectively, at the time point of 30 min, indicating inferior ability to reduce IFT. It is worth noting that, 92-U-A and 100-U-G did not reach equilibrium during 30 min of the analysis, whereas the IFT values for most of the peptides levelled off within the first 5 min. Besides these two peptides, 99-U-G reached an equilibrium around 20 min starting at 22.0 and ending at 11.8 mN/m. The slow adsorption of these peptides at the oil–water interface could be due to the long amino acid chain for these peptides (28–29 AAs), which might hinder diffusion. Furthermore, these peptides were also noted to be poorly soluble (Table 2), which could be the reason for slow adsorption as the peptides need to disassemble from their aggregated forms, diffuse and adsorb at the interface. Apart from longer AA sequence and lower solubility of the peptides, low *in situ* amphiphilicity could be another reason for the slow movement and adsorption kinetics; although 99-U-G and 100-U-G had high amphiphilic scores as 4.82 and 4.54, respectively. Nevertheless, 99-U-G reached IFT levels as low as CAS at 30 min.

98-U-B decreased the oil–water IFT to the same extent as CAS (11.8 mN/m), even though it is a long peptide (29 AAs) and its amphiphilic score is not very high (3.25). This is contradicting the results indicating

Table 2

Solubility (0.02 wt%) and pH of the peptides in buffer, and pH, observations for physical stability (CI and OI are indexes for creaming and oil rich phase accumulation on top, respectively. PS and OL encodes 'phase separation' and 'oil layer on top', respectively), surface weighted mean diameter D[3,2], and zeta potential of the emulsions stabilized with peptides or sodium caseinate (CAS) during storage.

Emulsion/sample code	Aqueous phase		Emulsion								Zeta potential (mV)
	pH	Solubility	pH	Observations on physical stability*			D[3,2] (μm)**				
			Day 0	Day 0	Day 1	Day 6	Day 0	Day 1	Day 3	Day 6	Day 1
80-S-A	5.73	Cloudy	5.99	–	–	OI=1	$0.38\pm0.06^{a,w}$	0.35 ± 0.05^{a}	0.27 ± 0.02^{a}	0.33 ± 0.09^{a}	37.8 ± 2.9
81-S-A	5.82	Soluble	5.96	–	OL, CI=1	PS	0.25 ± 0.22^{w}	–	–	–	-12.8 ± 2.5
82-S-A	5.20	Soluble	5.58	–	–	OI=2	$0.17\pm0.00^{a,w}$	0.51 ± 0.16^{b}	0.36 ± 0.07^{ab}	0.33 ± 0.01^{ab}	-53.7 ± 2.9
83-S-B	5.50	Soluble	5.53	–	–	–	$0.21\pm0.02^{a,w}$	0.27 ± 0.07^{a}	0.24 ± 0.05^{a}	0.29 ± 0.04^{a}	5.23 ± 2.0
84-S-B	5.37	Soluble	5.79	–	–	OI=1	$0.29\pm0.03^{a,w}$	0.26 ± 0.04^{a}	0.22 ± 0.02^{a}	0.22 ± 0.01^{a}	-71.8 ± 3.5
85-S-B	5.82	Soluble	5.89	–	–	–	$0.25\pm0.02^{a,w}$	0.25 ± 0.04^{a}	0.20 ± 0.02^{a}	0.21 ± 0.04^{a}	29.4 ± 3.3
86-S-B	5.41	Cloudy	5.74	–	–	OI=2	$0.22\pm0.00^{ab,w}$	0.24 ± 0.03^{b}	0.19 ± 0.02^{ab}	0.18 ± 0.02^{a}	-74.4 ± 2.8
87-S-G	5.82	Cloudy	5.93	PS	PS	PS	–	–	–	–	-15.9 ± 3.8
88-S-G	5.44	Cloudy	5.68	CI=5	CI=5	CI=5	$6.15\pm0.32^{a,y}$	5.76 ± 0.22^{a}	5.32 ± 0.15^{a}	5.79 ± 0.58^{a}	-19.2 ± 4.1
89-S-G	6.04	Cloudy	6.18	CI=5	CI=5	CI=5	$7.08\pm0.15^{b,y}$	6.80 ± 0.23^{b}	6.60 ± 0.04^{ab}	5.46 ± 0.81^{a}	-20.5 ± 1.5
90-S-G	5.24	Cloudy	5.52	CI=5	CI=5	PS	$5.49\pm3.44^{a,xy}$	7.79 ± 3.21^{a}	20.98 ± 17.9^{a}	–	-28.5 ± 8.1
91-S-G	4.93	Cloudy	5.37	–	–	PS	–	–	–	–	-28.8 ± 13.7
92-U-A	6.19	Cloudy	6.16	CI=5	CI=5	CI=5	27.96 ± 2.72^{z}	–	–	–	-10.2 ± 1.4
93-U-A	5.97	Soluble	6.05	CI=5	CI=5	CI=5	–	–	–	–	-9.7 ± 0.6
94-U-A	5.36	Soluble	5.42	CI=5	CI=5	CI=5	6.63 ± 2.11^{y}	11.0 ± 8.25	–	–	-22.4 ± 2.8
95-U-A	5.75	Cloudy	5.88	CI=3	CI=4	CI=4	$2.81\pm0.77^{a,wxy}$	3.65 ± 1.19^{a}	1.90 ± 0.64^{a}	3.05 ± 0.94^{a}	-47.7 ± 3.2
96-U-B	6.02	Soluble	5.81	–	OI=1	OI=1	$0.42\pm0.02^{ab,w}$	0.39 ± 0.02^{a}	0.47 ± 0.04^{ab}	0.5 ± 0.03^{b}	33.8 ± 2.6
97-U-B	5.56	Soluble	5.57	–	–	–	$0.20\pm0.00^{a,w}$	0.22 ± 0.01^{a}	0.18 ± 0.00^{a}	0.21 ± 0.04^{a}	25.2 ± 1.9
98-U-B	6.11	Cloudy	6.07	CI=2	CI=4	CI=5	$0.87\pm0.27^{a,wx}$	0.80 ± 0.25^{a}	1.17 ± 0.40^{a}	1.54 ± 1.38^{a}	5.2 ± 1.3
99-U-G	6.13	Cloudy	6.19	OI=3	OI=3	OI=3	$2.98\pm0.80^{b,wxy}$	2.48 ± 0.37^{ab}	2.22 ± 0.47^{ab}	1.28 ± 0.45^{a}	-42.3 ± 3.9
100-U-G	5.71	Cloudy	5.77	CI=5	CI=5	CI=5	$6.59\pm5.08^{a,y}$	8.94 ± 0.17^{a}	5.86 ± 0.75^{a}	6.37 ± 2.63^{a}	-15.5 ± 1.8
101-U-G	4.88	Cloudy	–	OL	PS	PS	–	–	–	–	-9.8 ± 0.6
102-U-G	5.75	Soluble	6.08	PS	PS	PS	–	–	–	–	-9.8 ± 0.6
103-U-G	6.15	Soluble	6.32	–	OI=2	OI=2	$0.63\pm0.14^{a,wx}$	0.62 ± 0.02^{a}	0.55 ± 0.17^{a}	0.57 ± 0.05^{a}	38.7 ± 2.7
104-P-G	5.72	Soluble	5.98	–	–	–	$0.21\pm0.04^{a,w}$	0.18 ± 0.03^{a}	0.18 ± 0.04^{a}	0.17 ± 0.01^{a}	-60.9 ± 3.0
105-P-G	5.90	Soluble	5.89	–	–	–	$0.18\pm0.00^{a,w}$	0.17 ± 0.88^{a}	0.17 ± 0.00^{a}	0.16 ± 0.00^{a}	-59.3 ± 2.5
106-P-A	5.19	Soluble	–	PS	PS	PS	–	–	–	–	–
107-P-A	4.75	Soluble	5.12	–	OL, CI=2	PS	0.34 ± 0.07^{w}	–	–	–	-46.5 ± 6.5
CAS	6.46	Soluble	6.50	–	–	–	$0.43\pm0.02^{ab,w}$	0.44 ± 0.06^{ab}	0.33 ± 0.05^{a}	0.47 ± 0.02^{b}	-40.7 ± 1.7

*Number codes 1, 2, 3, 4, and 5 stands for CI and OI being in the range of 0–10, 10–20, 20–30, 30–40, and + 40%. '-' indicates no creaming.

**Statistical differences between storage days are shown with the letters 'a' and 'b' and the differences between samples at day 0 are shown with the letters 'w', 'x', 'y', and 'z' (p < 0.05).

higher surface activity for middle length β-peptides (García-Moreno, Gregersen et al., 2020). However, it should be borne in mind that 98-U-B was not totally soluble, thus potential deformation of droplet shape by insoluble peptide particles might have occurred leading to a lower IFT. Interestingly, 93-U-A, which is a shorter peptide (16 AAs), had one of the lowest amphiphilic scores (2.36) among the assayed peptides, was better at decreasing the oil–water IFT (11.0 mN/m) than CAS. This result is similar to the findings reported by (García-Moreno, Gregersen et al., 2020), which indicate better reduction of oil–water IFT of α-peptides with a length of >18AAs. 94-U-A and 96-U-B had slightly higher IFT values (12.5 and 12.9 mN/m, respectively) compared to CAS, which may indicate a promising emulsifying activity for these peptides as well. These peptides have 26 AAs and high amphiphilic scores (4.68 and 4.16, respectively). On the other hand, peptides 95-U-A, 97-U-B, 102-U-G, and 103-U-G moderately decreased the oil–water IFT with equilibrium values between 15.8 and 18.2 mN/m at 30 min.

3.3.3. Potato-derived peptides

106-P-A and 107-P-A are truncated variants of the patatin-derived peptides α10 (29 AAs) and α12 (19 AAs), respectively, which were previously reported to have good emulsifying activities (García-Moreno, Gregersen et al., 2020). Nevertheless, both 106-P-A and 107-P-A displayed low interfacial activity (>20 mN/m). The low activity observed may be related to their shorter length (16 and 12 AAs, respectively) and thus inability to adopt a stable amphiphilic α-helix at the interface. Moreover, both variants lack the C-terminal domain found in α-10 and α-12, which corresponds to a large proportion of the helical structure in the native protein (Fig. S2). The lack of the C-terminal domain also

explains their low scores (<2) which is good agreement with the low activity.

104-P-G and 105-P-G are variants of γ1 (28 AAs), which was shown to be very good emulsifier and reduced oil–water IFT considerably (García-Moreno, Jacobsen et al., 2020). Superior surface-activities of 104-P-G and 105-P-G (Fig. 1C) were close to the findings of c, which reported lower IFT when γ-peptides were longer than 18 AAs, although 105-P-G is only 17 AAs. These results indicate the potential as emulsifiers for the two potato peptides. It is worth mentioning that the amphiphilic scores for these peptides were modest (3.69 and 2.45), which indicate that cumulative amphiphilicity, as calculated in EmulsiPred, does not alone appear to totally describe the emulsifying potential of peptides.

3.4. Physical stability of emulsions

3.4.1. Appearance of aqueous phase and pH

Solubility of the peptides in the aqueous phase has an influence on the emulsifying activity of the peptides (Ralet & Guéguen, 2000). Having the peptides dissolved in the buffer before the homogenization process allows the emulsifier peptides to rapidly diffuse towards the oil–water interface projecting their hydrophobic and hydrophilic sites to the oil and water phases, respectively. Table 2 shows the solubility of the peptides. Some of the peptides (13 out of 28) had a cloudy appearance, which indicates that those peptides were not totally soluble in the buffer used, and that partial aggregation or self-assembly occurred, as described above. Peptides when dissolved in buffer had pH values ranging from 4.75 to 6.15. The variation in the pH depends on the AA
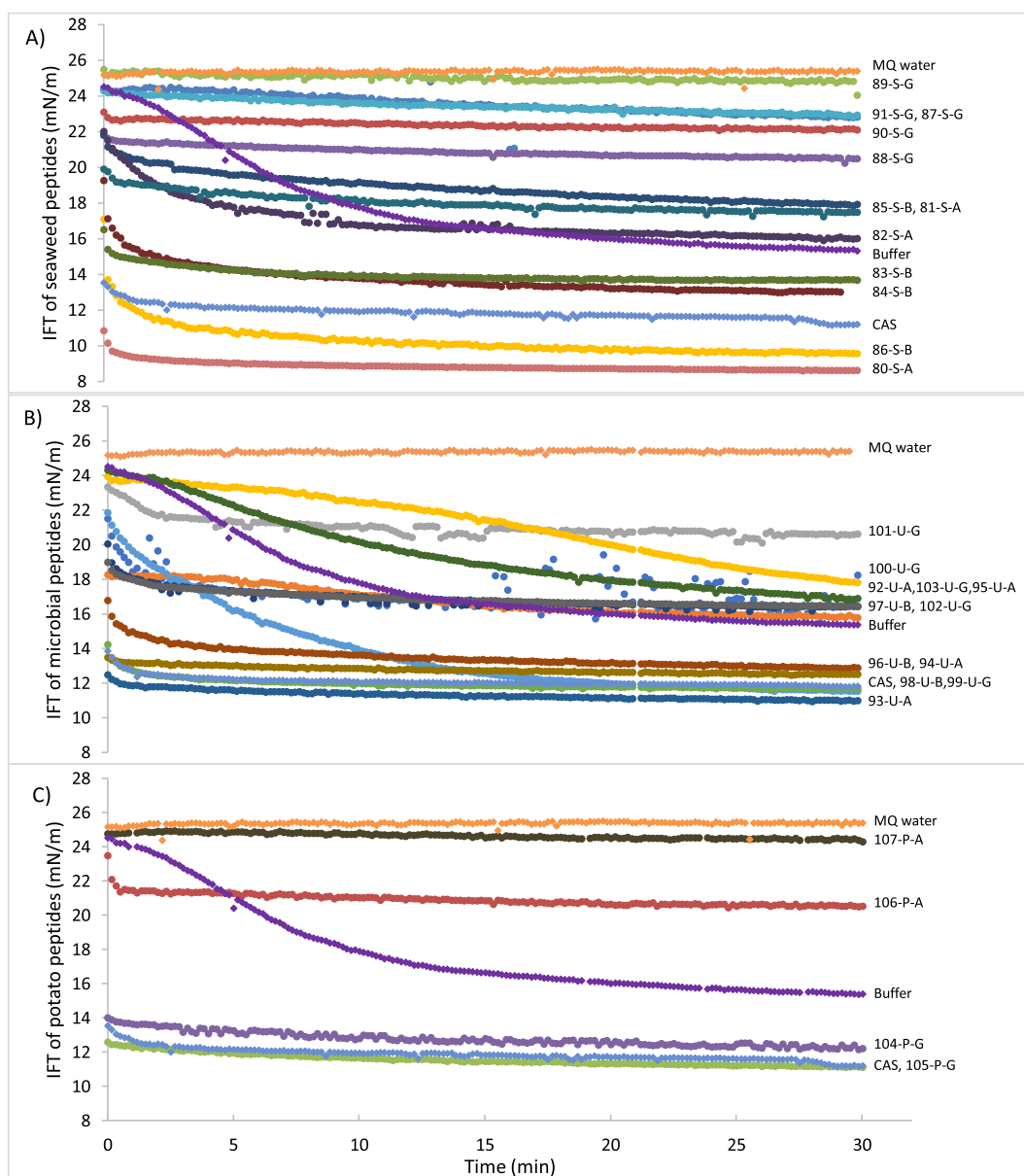
Fig. 1. Interfacial tension (mN/m) of A) seaweed, B) microbial, C) potato peptides, and control samples (MQ water, buffer, and sodium caseinate - CAS) as a function of time (min).

profile as well as acidic impurities present in the synthetic peptides used. In addition to the influence on the pH, impurities may potentially affect the observed properties to some degree. For screening and assessment of bioactive and functional properties, peptide purity varies in the literature from >70% to >98%, depending particularly on the specific functionality (Perez Espitia et al., 2012; Thery & Arendt, 2018). As no systematic studies, to the best of our knowledge, have been performed to assess the extent nor the nature of impurities, we cannot explicitly dismiss that divergence in emulsifying properties may be observed at higher purities. Here, we adhere to recent studies where > 70% was indeed regarded sufficient to evaluate peptide emulsifying properties (García-Moreno, Gregersen et al., 2020; García-Moreno, Jacobsen et al., 2020). In addition, peptides of > 70% purity gives significantly more reliable data compared to e.g. peptides identified in fractionated, albeit still complex, protein hydrolysates, which is commonly encountered throughout the literature as sufficient proof of peptide activity or function. Arguably, if deep and accurate characterization of e.g. peptide molecular structure is desired, a higher peptide purity would be needed.

3.4.2. Creaming and oil rich phase accumulation on top

After the production of the emulsions, physical stability was assayed during 6 days of storage (Table 2). One of the main indications for physical instability for the emulsions was creaming, as evaluated by CI. Creaming describes the movement of oil droplets upwards because of gravitational separation leaving a clear water phase in the bottom. 88-S-G, 89-S-G, 90-S-G, 92-U-A, 93-U-A, 94-U-A, and 100-U-G suffered from severe creaming instability (CI>40%) already at day 0. 98-U-B had creaming index increasing gradually after production during storage and reached a high level (CI>40%) at day 6. It is worth mentioning that these peptides have a low charge at pH 7 (absolute value of net charge at pH 7≤1.1), which may indicate insufficient repulsion between oil droplets (see section 3.4.4). Another indication for physical instability for these emulsions was the measured OI, where an oil rich phase accumulated on top of the emulsions, leaving a non-transparent water phase (with smaller oil droplet) in the bottom.

Several emulsions displayed oil rich phase accumulation on top at a reasonable level (OI<20%), and only one peptide, 99-U-G, resulted in an

OI higher than 20% (Table 2). This could be explained by the slow adsorption of the peptides at the oil–water interface as discussed in section 3.3. This presumably resulted in coalescence of the oil droplets before they were fully covered by peptide, thus leading to larger oil droplets, which moved to the top of the emulsion. Furthermore, some of the emulsions (81-S-A, 101-U-G, and 107-P-A) had an oil layer on top. This physical destabilization phenomenon is different from OI. The existence of an oil layer indicates the accumulation of oil after the breakage of the oil–water interfacial layer, also known as 'oiling-off' (McClements, 2016). This leads to upward movement of the free oil towards the top due to its lower density than the surrounding emulsion. These samples resulted in phase separation, which infers physical instability. This is in line with the high IFT values obtained for these peptides ranging between 17.5 and 24.3 mN/m (Fig. 1). Emulsions with no observable physical instability were 83-S-B, 85-S-B, 97-U-B, 104-P-G, 105-P-G, and CAS (Table 2), which were considered physically stable emulsions. Some of these peptides resulted in relatively high IFT values at 30 min. Therefore, there is no apparent relationship between physical stability and low IFT values. Indeed, low IFT only facilitates droplet breakup during emulsification, while physical stability of emulsions is mostly determined by the potential steric hindrance and/or electrostatic repulsions provided by the peptides adsorbed at the surface of the oil droplets (Berton-Carabin et al., 2018).

3.4.3. Zeta potential and droplet size

Zeta potential of the emulsions produced with peptides provided information about the surface charge of the peptide interfacial layer (Table 2). Peptides provide positive charge around oil droplets below their isoelectric point and negative charge above it. Isoelectric point (pI) and net charge of the peptides at pH 7 are shown in Table 1. Table 2 shows that the pH values of the emulsions ranged between 5.12 and 6.32. In emulsions with a pH value around the peptide's isoelectric point, the peptides have an overall charge around zero, meaning that there are equally charged AAs both negatively and positively (McClements, 2016). Overall, zeta potential values of the emulsions ranged between -74 to 39 mV, which is comparable to the results reported in other studies, where peptides were used as the only emulsifiers, with values varying between -78 to 35 mV and -62 and -14 mV (García-Moreno, Gregersen et al., 2020; García-Moreno, Jacobsen et al., 2020).

Droplet size of the emulsions provides information about the emulsifying ability of the peptides. During homogenization, the peptide adsorption speed determines the minimum droplet size that can be obtained (i.e., the faster the adsorption rate, the droplet disruption is facilitated and smaller droplet sizes can be achieved) (McClements, 2016). Table 2 shows the surface weighted mean diameter (D[3,2]) of the emulsions stabilized with peptides or CAS during storage. The missing values correspond to the samples that did not form emulsion or had phase separation at the specific time of storage. Overall, results of D[3,2] indicated that most of the emulsions stabilized with the peptides were not significantly different than the emulsion stabilized with CAS at day 0. Peptides that provided emulsions with larger D[3,2] values compared to CAS were 88-S-G, 89-S-G, 90-S-G, 92-U-A, 94-U-A, and 100-U-G, which were also observed with severe creaming (Table 2). Similarly, volume weighted mean dimeter, D[4,3] (Table S3), show that even more peptides performed similar to CAS at day 0 (Table S3). Only 92-U-A and 95-U-A had significantly larger D[4,3] values compared to the control at day 0 (p<0.05).

Emulsions produced with the peptides 80-S-A, 82-S-A, 84-S-B, 86-S-B, 95-U-A, 96-U-B, 99-U-G, 103-U-G, 104-P-G, 105-P-G, 107-P-A or CAS had high absolute surface charge (>30 mV), which may indicate a better physical stability provided by the strong electrostatic repulsion between oil droplets (McClements, 2016). In line with this, the emulsions produced with the above-mentioned peptides also had smaller or similar D[3,2] values, which ranged between 0.17 and 2.98 μm, compared to CAS (0.43±0.02 μm) at the day of emulsion production (p<0.05). Furthermore, these samples were physically stable during 6 days of storage

except the emulsions stabilized with 99-U-G and 107-P-A (Table 2).

3.4.3.1. Seaweed-derived peptides.
Except for two peptides (87-S-G and 91-S-G), all seaweed peptides were able to stabilize fish oil-in-water emulsions (Table 2), although emulsions stabilized with 81-S-A and 90-S-G destabilized after 1 and 6 days of storage, respectively. The four above-mentioned peptides all displayed low IFT reduction (17.5–22.9 mN/m at 30 min), also denoting poor surface activity. Two emulsions produced with γ-peptides (88-S-G and 89-S-G) had larger D[3,2] values (6.15 and 7.08 μm) compared to the emulsions produced with α- and β-peptides, which had sizes ranging between 0.17 and 0.38 μm at day 0. Likewise, low zeta potential for the emulsions stabilized with 88-S-G and 89-S-G (-19 and -21 mV, respectively) is associated with the severe creaming observed for the emulsions (CI>40%, Table 2). 82-S-A, 84-S-B, and 86-S-B had high absolute surface charge (>30 mV), which indicates a better physical stability provided by the strong electrostatic repulsion between oil droplets (McClements, 2016), which was supported by the stable D[3,2] values during storage. However, these emulsions had oil rich phase accumulation on top (OI<20%), and although this does not relate directly to D[3,2] results, D[4,3] values had high standard deviation (Table S3) indicating both polydispersity and variability between replicates for measurements.

Emulsions produced with the 83-S-B and 85-S-B displayed high physical stability based on the observations of creaming and oil accumulation as well as droplet size distribution during storage, in spite of low absolute zeta potential values (<30 mV). They had 25 and 20 AAs, respectively, which were longer than the best emulsifier β-peptides length range (13–15 AAs) suggested in a previous study (García-Moreno, Gregersen et al., 2020). Although these peptides were mediocre at decreasing oil–water IFT (13.7–17.9 mN/m at 30 min, Fig. 1), they had good solubility in buffer, good physical stability and relatively small D[3,2] values compared to CAS (Table 2) during storage. Furthermore, secondary structure of these peptides were predicted to be β-strand, which is reported to provide stiffer interfaces compared to peptides adopting α-helix conformation at the interface (García-Moreno et al., 2021)

3.4.3.2. Methanotrophic bacteria-derived peptides.
Nine emulsions (out of 12) produced with microbial peptides formed an emulsion at day 0, and six of them had stable D[3,2] values during 6 days of storage. 99-U-G showed a decrease in the D[3,2] and D[4,3] values, which was presumably related to the largest OI (>20%) among all the emulsions even at day 0. As mentioned previously (sections 3.3.2 and 3.4.2), 99-U-G had slow adsorption at the oil–water interface (Fig. 1B), and therefore led to an emulsion with poor physical stability with high oil index. In addition, poor solubility of the peptide in the buffer might have led to an insufficient emulsifying activity. Emulsions produced with the peptides 92-U-A and 94-U-A had severe creaming (CI>40%). Indeed, 92-U-A was intermediate at decreasing oil–water IFT (16.9 mN/m at 30 min) and had one of the lowest amphiphilic score (2.45) among other peptides as well as a low zeta potential (-10 mV). In contrast, 94-U-A was able to decrease the oil–water IFT down to 12.5 mN/m and had a high amphiphilic score of 4.68, but a low zeta potential (-22 mV) and thus inefficient electrostatic repulsion, indicates the importance of oil droplet surface charge for physical stability of emulsions.

D[3,2] values range between 0.20 and 6.59 μm for the stable emulsions produced with microbial peptides. Within these emulsions, 100-U-G had a significantly larger D[3,2] value compared to CAS, which explains its severe creaming instability (CI>40%), poor ability to decrease IFT (18.2 mN/m at 30 min). The close to zero net charge at pH 7 (Table 1) indicate insufficient electrostatic repulsion between oil droplets, as confirmed by a low zeta potential of -16 mV. In contrast, 97-U-B provided one of the smallest D[3,2], which was stable during storage. This was in line with its physical stability (Table 2) and high amphiphilic score (5.07). However, it was somewhat surprising based on the

mediocre reduction of the oil–water IFT (16.5 mN/m at 30 min) and the somewhat low zeta potential of 25 mV (<30 mV). Secondary structure and length (16 AAs) of 97-U-B could be the reason for its good emulsifying activity, which was suggested in a previous study for emulsifier β-peptides with a length in the range of 13–15 AAs (García-Moreno, Gregersen et al., 2020).

3.4.3.3. Potato-derived peptides. Only three emulsions (out of 4) could be produced when using the assayed potato peptides as emulsifier. 104-P-G and 105-P-G, which are the variants of the highly emulsifying peptide γ1 (García-Moreno, Gregersen et al., 2020; García-Moreno, Jacobsen et al., 2020), provided smaller D[3,2] values than CAS at day 0. The D[4,3] values of emulsions produced with 104-P-G and 105-P-G at day 6 were comparable to the D[4,3] value obtained for γ1 in a previous study (García-Moreno, Gregersen et al., 2020). These γ1 variants did not show any physical instability during storage and resulted in highly negative zeta potential values. Although a generally higher emulsifying activity was reported for the γ-peptides longer than 18 AAs (García-Moreno, Gregersen et al., 2020), 105-P-G (17 AAs) did not show inferior emulsifying activity compared to 104-P-G (25 AAs). This again indicates that no single parameter, e.g. peptide length or cumulative amphiphilicity, can be used as a governing property for emulsifying potential, and factors such as *in situ* interfacial conformation play a very important role.

106-P-A did not form an emulsion and 107-P-A had physical instabilities after production (Table 2). This was however expected based on amphiphilic scores <2. Although 107-P-A was able to form an emulsion with low D[3,2], it had creaming and oil layer accumulation on top of the emulsion on day 1 and displayed phase separation towards the end of the storage (Table 2). This clearly shows that high zeta potential (−47 mV) is not merely enough for obtaining a stable emulsion. Although length appears to be of importance for peptides adopting α-helical conformation at the interface, the missing C-terminal domain described in section 3.3.3 is likely also a key factor in the inferior properties observed for the truncated variants.

3.5. Principle component analysis and selection of best performing emulsifier peptides

PCA showed that the first four components explained 84% of the variability in the original data (Fig. 2). First principle component was described by the molecular weight and length of the peptides followed by D[4,3], zeta potential, D[3,2], and pI, explaining 36% of the variability in the original data. Second principle component was largely described by IFT followed by zeta potential and accounted for 21% of the variability in the data. Third principle component explained variation in pI and D[3,2] followed by D[4,3] and IFT, explaining 14% of the variation. Lastly, fourth principle component explained 13% of the variance and was defined largely by the amphiphilic score.

Emulsions with a larger surface charge are located on the upper left side of the plot. Both droplet size mean diameters were located on the right side of the plot indicating that both surface and volume weighed mean diameters have a similar trend and the emulsions with smaller droplets are located on the left side of the plot. IFT did not have any direct correlation with any of the other variables. Even though IFT and amphiphilic score are related, there are other factors affecting the IFT such as solubility and size of the peptide, which is affecting diffusion; therefore, these two variables were not negatively correlate in the biplot. Nevertheless, peptides with low IFT indicating their ability to decrease the oil–water IFT in a large extent are located on the upper part of the plot. Considering the location of the variables and distribution trend of the peptides altogether, peptides (82-S-A, 84-S-B, 86-S-B, 104-P-G, and 105-P-G) located in the upper left quadrant of the plot are indicating good emulsifying activities.

In addition to the above-mentioned overall analysis, some peptides providing outstanding results in certain parameters were also selected as good emulsifiers even though they were not located at the upper-left quadrant of the biplot. On the other hand, some peptides were located closer to the upper-left quadrant; however, emulsions experienced physical instability. For example, even though 94-U-A and 99-U-G performed well in decreasing oil–water IFT, they had high degree of CI or OI, indicating poor emulsifying activity. Likewise, 81-S-A, 88-S-G, 90-S-G, and 94-U-A showed high creaming instability (CI>40%) and/or resulted in phase separation during the 6 days of storage and low zeta potential (<30 mV), indicating higher likelihood of physical instability. Therefore, these peptides were not considered as good emulsifiers. On the contrary, 85-S-B did actually have good physical stability during storage; however, it had zeta potential lower than 30 mV and was not efficient in decreasing the oil–water IFT. Therefore, it was not selected. Similarly, 83-S-B had good physical stability, small droplet size and decreased IFT which made it a good candidate as an emulsifier. 97-U-B did not decrease the IFT between oil and water sufficiently; however, it provided very good physical stability in emulsion; therefore, it was selected as one of the good emulsifier peptides. Similarly, 80-S-A and
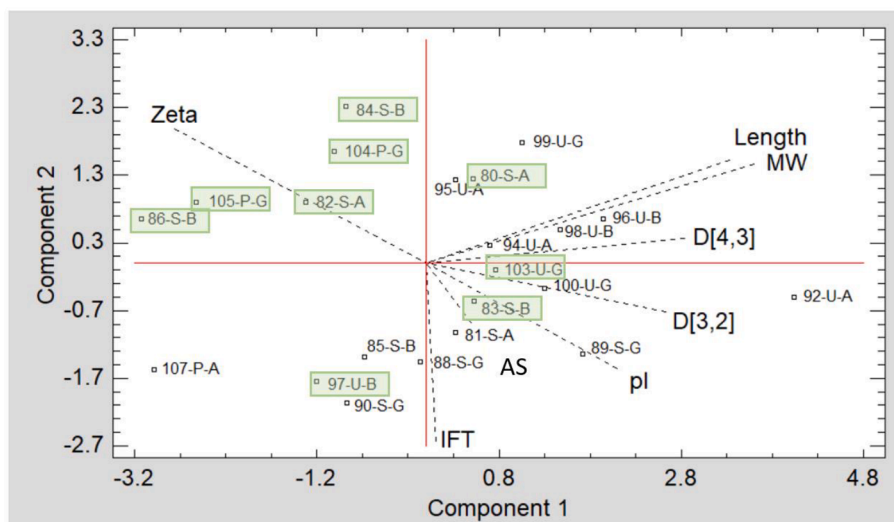

Fig. 2. Principle component analysis (PCA) biplot. Green highlighted peptides that were selected as good emulsifiers. Zeta, MW, D[3,2], D[4,3], pI, AS, and IFT abbreviations on the biplot were used for zeta potential, molecular weight, surface weighed mean diameter, volume weighed mean diameter, isoelectric point, amphiphilic score and IFT, respectively. (For interpretation of the references to color in this figure legend, the reader is referred to the web version of this article.)

103-U-G had small and stable droplet size, low CI (≤2) and absolute zeta potential higher than 30 mV, and thereby selected as good emulsifiers.

Verified *in vitro* functionality of isolated peptides provide additional knowledge about structure/function relationship of emulsifier peptides as well as insight into the potential hidden gems in food proteins. Nevertheless, this may not be directly transferable to the properties observed for a large-scale hydrolysate, as these are highly complex and contain thousands of peptides (Jafarpour et al., 2020). However, pre-liminary investigations on potato protein hydrolysates do show that applying a designed hydrolysis for targeted release of verified peptide emulsifiers does not only release the intended peptides but also show improved bulk functionalities of the hydrolysate when compared to hydrolysates produced with other industrially relevant proteases (manuscript in preparation).

3.6. Protein modelling and putative peptide structure

Templated homology modelling has proven highly beneficial to gain insight into the secondary structure of the peptides, which affects their emulsification properties (García-Moreno, Gregersen et al., 2020). For instance, we previously hypothesized that a emulsifier peptide identified by bioinformatics (γ1) was likely a facial emulsifier as it originates from a partially buried, amphiphilic surface α-helix (García-Moreno, Jacobsen et al., 2020). The helical conformation at the interface has subsequently been confirmed by synchrotron radiation circular dichroism (García-Moreno et al., 2021). Using the approach, we visualized the nine selected peptides within a structural model of their native proteins (Fig. 3A).

In all cases, the best fitting model, which spans the target peptide, was selected to visualize the putative peptide structure. In the case of Q60B76 (103-U-G), no satisfactory model was obtained, and thus no structural information could be extracted. Quality parameters in terms of sequence identity, GMQE (Waterhouse et al., 2018), and QMEAN (Studer et al., 2020) are summarized in Table 3 and the local quality estimates are found in Fig. S3 for the selected models. Model quality assessment is further elaborated in the Supplementary Information.

Using the modelled structures, we were able to determine the putative content of secondary structural elements for the peptides (Table 3). One of the α-type peptides, 82-S-A, (as well as the two γ-type from patatin (104-P-G and 105-P-G)), are predominantly α-helical. Furthermore, two of the β-type (86-S-B and 97-U-B) are predominantly β-strand. 80-S-A and 84-S-B contains significant amounts of both structural elements. It is widely accepted that isolated peptides may partake a very different conformation than they do in their native protein (Hanazono et al., 2018). Nevertheless, a recent study by García-Moreno et al. (2021) found that the oil/water interfacial structure of emulsifier peptides is comparable to the native conformation, if the peptide is found in a surface exposed region of the protein. In all cases, the peptides appear to be surface exposed (Fig. 3A), and the local environments can hence, to some extent, be regarded similar to the oil–water interface. Consequently, the modelled structures may be regarded as probable homologues to the peptide interfacial structure.

Considering the putative peptide structures (Fig. 3A) and the distribution of hydrophobic and hydrophilic amino acids (Fig. 3B), it is evident why the peptides were both predicted and performed as good emulsifiers. In a previous study, it was shown that secondary structure, length, and pI of peptides all influence the interfacial properties (e.g., structure, viscoelasticity, and charge) and thereby physical stability of the emulsions by offering steric hindrance and electrostatic repulsions between oil droplets (García-Moreno et al., 2021). For α-helical peptides, it is a prerequisite to have both a hydrophobic and a hydrophilic face (Eisenberg et al., 1982), which is obtained by a beneficial AA distribution along the 3.4 residues involved in each turn. This type of distribution is recognized in both 80-S-A and 82-S-A as well as 104-P-G and 105-P-G, which are derivatives of γ-1 (García-Moreno, Jacobsen et al., 2020), shown to be α-helical at the oil–water interface (García-Moreno
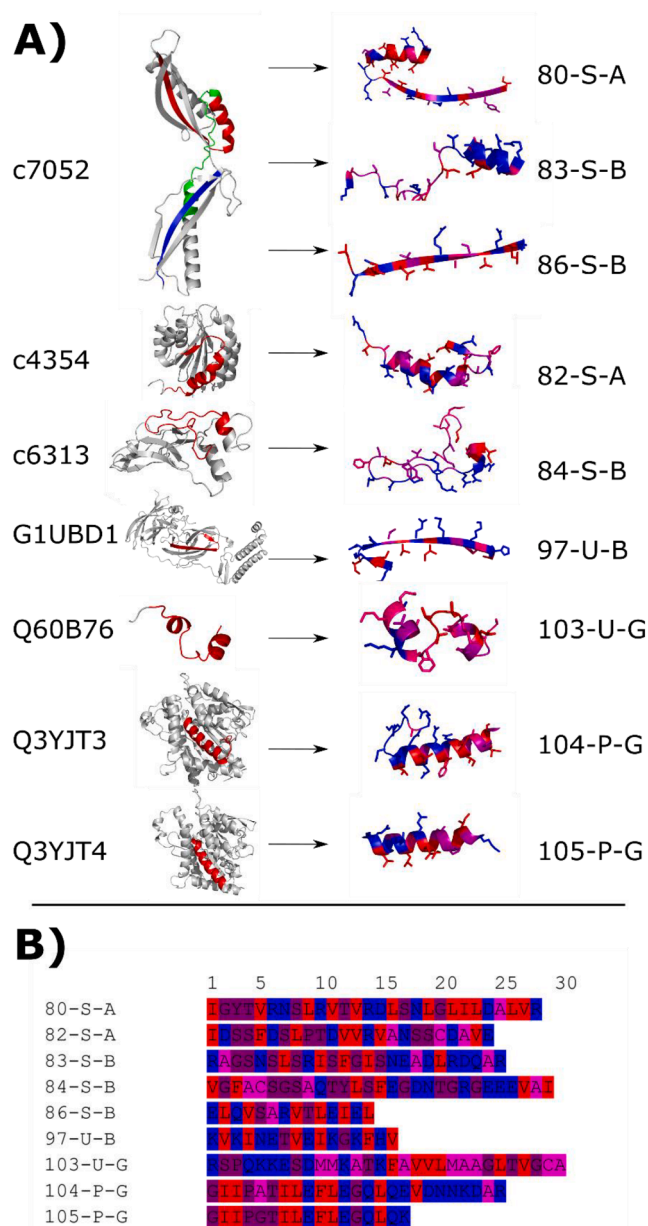

Fig. 3. A) Modelled protein structures with highlighted peptides in red (for c7052, 80-S-A is red, 83-S-B is green, and 86-S-B is blue) and the structure of the isolated peptide with visible side chains and colored according to the Swiss-Model color scheme: Residues are depicted as very hydrophilic in blue, partially hydrophilic in purple, partially hydrophobic in pink, and very hydrophobic in red. B) Peptide sequences according to the Swiss-Model color scheme: to illustrate hydrophobic/hydrophilic distribution in a linear manner. (For interpretation of the references to color in this figure legend, the reader is referred to the web version of this article.)

et al., 2021). This may clarify the discussion in section 3.4.3 regarding the good emulsifying activity of 105-P-G despite its shorter length. The good emulsifying activity of the shorter variant of γ1 could be explained by the superior emulsifying activity reported for α-helical peptides comprising at least three helical turns, corresponding to 11 AAs (Enser et al., 1990).

For β-strand peptide emulsifiers, the prerequisite for a hydrophobic and a hydrophilic face is alternating hydrophobic and hydrophilic amino acids (Dexter & Middelberg, 2008). This distribution is very clearly seen in for instance 86-S-B throughout the peptide and also to a very large degree in 97-U-B. Both peptides are also modelled to be

Table 3
Summary of model quality parameters for all modelled peptides along with their native protein accession, position, template STML ID. Content of secondary structural elements was based on the models as depicted in the Swiss-Model Workspace. NA: Not applicable, based on the model not spanning the full peptide and the very poor model quality.

Peptide	Protein	Position	Template	Identity	GMQE	QMEAN	% α-helix	% β-strand
80-S-A	c7052_g1_i1.p1	105–133	4hvz.1.M	34.1%	0.65	−2.99	46%	46%
82-S-A	c4354_g1_i1.p1	191–215	4ihk.1.A	16.8%	0.31	−3.23	58%	13%
83-S-B	c7052_g1_i1.p1	132–157	4hvz.1.M	34.1%	0.65	−2.99	40%	8%
84-S-B	c6313_g1_i1.p1	72–101	3nkg.1.A	27.6%	0.32	−5.03	31%	24%
86-S-B	c7052_g1_i1.p1	212–226	4hvz.1.M	34.1%	0.65	−2.99	0%	86%
97-U-B	G1UBD1	58–74	3rgb.1.A	100%	0.97	−0.84	0%	81%
103-U-G	Q60B76	6–36	3woa.1.A	8.0%	0.22	−4.67	NA	NA
104-P-G	Q3YJT3	29–54	4pka.1.A	88.2%	0.95	−0.66	72%	0%
105-P-G	Q3YJT4	29–46	4pka.1.A	89.6%	0.95	−0.94	100%	0%

almost fully, undisturbed β-strands (Fig. 3A), comprising 86% and 81% β-strand, respectively (Table 3). In addition, their length correspond very well the optimal size range for β-strand peptides (García-Moreno, Gregersen et al., 2020). The distribution of β-strands is less evident in 83-S-B and 84-S-B, although they do contain regions of alternating hydrophobic and hydrophilic amino acids (Fig. 3B).

For γ-type peptide emulsifiers, one end is hydrophobic and one end is hydrophilic, which can facilitate perpendicular interaction with the interphase (Dexter & Middelberg, 2008). This distribution is highly evident for 103-U-G, 104-P-G, and, to a lesser extent, 105-P-G (Fig. 3B). As the model for 103-U-G is particularly poor and the AA distribution does not correlate with the prerequisites for α-helical or β-strand emulsifiers, the interfacial structure is unclear and very hard to predict.

4. Conclusions

In this study, we successfully characterized the protein content of the biomass resulting from a mixed methotrophic fermentation process by bottom-up quantitative proteomics. Using the most abundant proteins from this and other proteomics studies, we were able to predict emulsifying peptides embedded in proteins from seaweed, methanotrophic bacteria, and potato with great success. Predicted peptides were synthesized and subjected to *in vitro* assays, where a high number of the predicted peptides showed better or comparable emulsifying activity to sodium caseinate in fish oil-in-water emulsions. The emulsifying activity of peptides varied based on their solubility, the ability of decreasing IFT, and structural characteristics such as length, isoelectric point, hydrophilic/lipophilic balance and putative conformation. Peptides predicted to partake α-helical structure were found to be more efficient when the length is sufficient to form helical structure, whereas peptides adopting β-strand were better emulsifiers at shorter lengths (14–16 AAs) where faster diffusion and less likelihood of aggregate formation played an important role. Out of 28 assayed peptides, nine were selected as good emulsifiers based on their *in vitro* emulsifying potential. All three analyzed protein sources were represented among the nine peptides, which are found in proteins constituting from 4 to 33% of the total protein content in industrially relevant raw materials and side-streams, thereby making them highly promising leads as large-scale obtainable food bioactives. This demonstrates the high potential and the strengths of applying a bottom-up strategy compared to traditional top-down approaches in the search for new bioactive peptides. Furthermore, based on the predicted emulsification mechanism and putative structure from template-based modelling, the nine peptides also represent different types of peptide emulsifiers, thereby making this study a valuable contribution for a deeper understanding of what constitutes a good peptide emulsifier.

CRediT authorship contribution statement

Betül Yesiltas: Conceptualization, Methodology, Investigation, Formal analysis, Visualization, Writing - original draft. **Simon Gregersen:** Conceptualization, Methodology, Investigation, Formal analysis, Visualization, Writing - original draft. **Linea Lægsgaard:** Formal analysis, Investigation. **Maja L. Brinch:** Formal analysis, Investigation. **Tobias H. Olsen:** Conceptualization, Formal analysis, Investigation. **Paolo Marcatili:** Conceptualization, Methodology, Formal analysis, Investigation. **Michael T. Overgaard:** Conceptualization, Funding acquisition, Supervision. **Egon B. Hansen:** Conceptualization, Funding acquisition, Project administration. **Charlotte Jacobsen:** Conceptualization, Funding acquisition, Project administration, Supervision, Writing - review & editing. **Pedro J. García-Moreno:** Conceptualization, Methodology, Supervision, Writing - review & editing.

Declaration of Competing Interest

The authors declare that they have no known competing financial interests or personal relationships that could have appeared to influence the work reported in this paper.

Acknowledgements

Appendix A. Supplementary data

Supplementary data to this article can be found online at https://doi.org/10.1016/j.foodchem.2021.130217.

References

Ashaolu, T. J. (2020). Antioxidative peptides derived from plants for human nutrition: Their production, mechanisms and applications. *European Food Research and Technology, 246*(5), 853–865. https://doi.org/10.1007/s00217-020-03479-y.

Asioli, D., Aschemann-Witzel, J., Caputo, V., Vecchio, R., Annunziata, A., Næs, T., & Varela, P. (2017). Making sense of the "clean label" trends: A review of consumer food choice behavior and discussion of industry implications. *Food Research International, 99*, 58–71. https://doi.org/10.1016/j.foodres.2017.07.022.

Berton-Carabin, C. C., Sagis, L., & Schroën, K. (2018). Formation, Structure, and Functionality of Interfacial Layers in Food Emulsions. *Annual Review of Food Science and Technology, 9*, 551–587. https://doi.org/10.1146/annurev-food-030117-012405.

Braig, K., Otwinowskitt, Z., Hegdett, H., Boisvert, D. C., Joachimiakt, A., Horwich, A. L., & Sigler Tt, P. B. (1994). The crystal structure of the bacterial chaperonin GroEL at 2.8 A Crystallization and structure determination. *Nature, 371*, 578–586.

Cheng, Y., Chen, J., & Xiong, Y. L. (2014). Interfacial Adsorption of Peptides in Oil-in-Water Emulsions Costabilized by Tween 20 and Antioxidative Potato Peptides. *Journal of Agricultural and Food Chemistry, 62*(47), 11575–11581. https://doi.org/10.1021/jf5038135.

Cheng, Y., Xiong, Y. L., & Chen, J. (2010). Antioxidant and emulsifying properties of potato protein hydrolysate in soybean oil-in-water emulsions. *Food Chemistry, 120* (1), 101–108. https://doi.org/10.1016/j.foodchem.2009.09.077.

Cox, J., & Mann, M. (2008). MaxQuant enables high peptide identification rates, individualized p.p.b.-range mass accuracies and proteome-wide protein quantification. *Nature Biotechnology, 26*(12), 1367–1372. https://doi.org/10.1038/nbt.1511.

Cui, H., Webber, M. J., & Stupp, S. I. (2010). Self-Assembly of Peptide Amphiphiles: From Molecules to Nanostructures to Bio materials. *Biopolymers, 94*(1), 392–406. https://doi.org/10.1002/bip.

Dexter, A. F., & Middelberg, A. P. J. (2008). Peptides as functional surfactants. *Industrial and Engineering Chemistry Research, 47*(17), 6391–6398. https://doi.org/10.1021/ie800127f.

Eisenberg, D., Weiss, R. M., & Terwilliger, T. C. (1982). *The helical hydrophobic moment : amphiphilicity of a helix., 299*(September), 371–374.

Enser, M., Bloomberg, G. B., Brock, C., & Clark, D. C. (1990). De novo design and structure-activity relationships of peptide emulsifiers and foaming agents. *International Journal of Biological Macromolecules, 12*(2), 118–124. https://doi.org/10.1016/0141-8130(90)90063-G.

Falade, E. O., Mu, T. H., & Zhang, M. (2021). Improvement of ultrasound microwave-assisted enzymatic production and high hydrostatic pressure on emulsifying, rheological and interfacial characteristics of sweet potato protein hydrolysates. *Food Hydrocolloids, 117*(February), Article 106684. https://doi.org/10.1016/j.foodhyd.2021.106684.

Feger, G., Angelov, B., & Angelova, A. (2020). Prediction of Amphiphilic Cell-Penetrating Peptide Building Blocks from Protein-Derived Amino Acid Sequences for Engineering of Drug Delivery Nanoassemblies. *Journal of Physical Chemistry B, 124*(20), 4069–4078. https://doi.org/10.1021/acs.jpcb.0c01618.

Findlay, B., Zhanel, G. G., & Schweizer, F. (2010). Cationic amphiphiles, a new generation of antimicrobials inspired by the natural antimicrobial peptide scaffold. *Antimicrobial Agents and Chemotherapy, 54*(10), 4049–4058. https://doi.org/10.1128/AAC.00530-10.

García-Moreno, P. J., Gregersen, S., Nedamani, E. R., Olsen, T. H., Marcatili, P., Overgaard, M. T., … Jacobsen, C. (2020). Identification of emulsifier potato peptides by bioinformatics: Application to omega-3 delivery emulsions and release from potato industry side streams. *Scientific Reports, 10*(1). https://doi.org/10.1038/s41598-019-57229-6.

García-Moreno, P. J., Jacobsen, C., Marcatili, P., Gregersen, S., Overgaard, M. T., Andersen, M. L., Sørensen, A.-D. M., & Hansen, E. B. (2020). Emulsifying peptides from potato protein predicted by bioinformatics: Stabilization of fish oil-in-water emulsions. *Food Hydrocolloids, 101*. https://doi.org/10.1016/j.foodhyd.2019.105529.

García-Moreno, P., Yang, J., Gregersen, S., Jones, N., Berton-Carabin, C. C., Sagis, L., … Jacobsen, C. (2021). The structure, viscoelasticity and charge of potato peptides adsorbed at the oil- water interface determines the physicochemical stability of fish oil-in-water emulsions. *Food Hydrocolloids, 115*, Article 106605.

Gregersen, S., Pertseva, M., Marcatili, P., Holdt, S. L., Jacobsen, C., García-Moreno, P. J., & Hansen, E. B. (2020). Proteomic characterization of pilot scale hot-water extracts from the industrial carrageenan red seaweed Eucheuma denticulatum. *bioRxiv*. https://data.mendeley.com/datasets/g45gbw5r7n/draft?a=4825cedd-67c9-481f-a844-55bf1f3e794f, (2021).

Hajfathalian, M., Ghelichi, S., García-Moreno, P. J., Moltke Sørensen, A. D., & Jacobsen, C. (2018). Peptides: Production, bioactivity, functionality, and applications. *Critical Reviews in Food Science and Nutrition, 58*(18), 3097–3129. https://doi.org/10.1080/10408398.2017.1352564.

Hanazono, Y., Takeda, K., & Miki, K. (2018). Co-translational folding of α-helical proteins: Structural studies of intermediate-length variants of the λ repressor. *FEBS Open Bio, 8*(8), 1312–1321. https://doi.org/10.1002/feb4.2018.8.issue-810.1002/2211-5463.12480.

Jacobsen, C. (2015). Some strategies for the stabilization of long chain n-3 PUFA-enriched foods: A review. *European Journal of Lipid Science and Technology, 117*(11), 1853–1866. https://doi.org/10.1002/ejlt.201500137.

Jafarpour, A., Gomes, R. M., Gregersen, S., Sloth, J. J., Jacobsen, C., & Moltke Sørensen, A. D. (2020). Characterization of cod (Gadus morhua) frame composition and its valorization by enzymatic hydrolysis. *Journal of Food Composition and Analysis, 89*(February), Article 103469. https://doi.org/10.1016/j.jfca.2020.103469.

Jafarpour, A., Gregersen, S., Gomes, R. M., Marcatili, P., Olsen, T. H., Jacobsen, C., … Sørensen, A. M. (2020). Biofunctionality of Enzymatically Derived Peptides from Codfish (Gadus morhua) Frame: Bulk In Vitro Properties, Quantitative Proteomics, and Bioinformatic Prediction. *Marine Drugs, 18*, 599. https://doi.org/10.3390/md18120599.

Kanehisa, M., & Goto, S. (2000). KEGG: Kyoto Encyclopedia of Genes and Genomes. *Nucleic Acids Research, 28*(1), 27–30. https://doi.org/10.3892/ol.2020.11439.

Larsen, E. B. (2002). U.S. Patent No. 6,492,135. Washington, DC: U.S. Patent and Trademark Office.

Matsumura, Y., & Matsumiya, K. (2012). Proteins – Peptides as Emulsifying Agents. In Navam S. Hettiarachchy (Ed.), Food Proteins and Peptides: Chemistry, functionality, interactions and commercialization (pp. 125–150).

McClements, D. J. (2016). *Food Emulsions: Principles, practices, and techniques*. CRC Press Taylor & Francis Group.

Minkiewicz, P., Iwaniak, A., & Darewicz, M. (2019). BIOPEP-UWM database of bioactive peptides: Current opportunities. *International Journal of Molecular Sciences, 20*(23). https://doi.org/10.3390/ijms20235978.

Myronova, N., Kitmitto, A., Collins, R. F., Miyaji, A., & Dalton, H. (2006). Three-dimensional structure determination of a protein supercomplex that oxidizes methane to formaldehyde in Methylococcus capsulatus (Bath). *Biochemistry, 45*(39), 11905–11914. https://doi.org/10.1021/bi061294p.

Olsen, T. H., Yesiltas, B., Marin, F. I., Pertseva, M., García-Moreno, P. J., Gregersen, S., … Marcatili, P. (2020). AnOxPePred: Using deep learning for the prediction of antioxidative properties of peptides. *Scientific Reports, 10*(1). https://doi.org/10.1038/s41598-020-78319-w.

Perez Espitia, P. J., de Fátima Ferreira Soares, N., dos Reis Coimbra, J. S., de Andrade, N. J., Souza Cruz, R., & Alves Medeiros, E. A. (2012). Bioactive Peptides: Synthesis, Properties, and Applications in the Packaging and Preservation of Food. *Comprehensive Reviews in Food Science and Food Safety, 11*(2), 187–204. https://doi.org/10.1111/j.1541-4337.2011.00179.x.

Poore, J., & Nemecek, T. (2019). Reducing food's environmental impacts through producers and consumers. *Science, 360*, 987–992. https://doi.org/10.1126/science.aaq0216.

Ralet, M. C., & Guéguen, J. (2000). Fractionation of Potato Proteins: Solubility, Thermal Coagulation and Emulsifying Properties. *LWT - Food Science and Technology, 33*(5), 380–387. https://doi.org/10.1006/fstl.2000.0672.

Schwanhäusser, B., Busse, D., Li, N.a., Dittmar, G., Schuchhardt, J., Wolf, J., … Selbach, M. (2011). Global quantification of mammalian gene expression control. *Nature, 473*(7347), 337–342. https://doi.org/10.1038/nature10098.

Shin, J.-B., Krey, J. F., Hassan, A., Metlagel, Z., Tauscher, A. N., Pagana, J. M., … Barr-Gillespie, P. G. (2013). Molecular architecture of the chick vestibular hair bundle. *Nature Neuroscience, 16*(3), 365–374. https://doi.org/10.1038/nn.3312.

Studer, G., Rempfer, C., Waterhouse, A. M., Gumienny, R., Haas, J., & Schwede, T. (2020). QMEANDisCo-distance constraints applied on model quality estimation. *Bioinformatics (Oxford, England), 36*(6), 1765–1771. https://doi.org/10.1093/bioinformatics/btz828.

Thery, T., & Arendt, E. K. (2018). Antifungal activity of synthetic cowpea defensin Cp-thionin II and its application in dough. *Food Microbiology, 73*, 111–121. https://doi.org/10.1016/j.fm.2018.01.006.

Tyanova, S., Temu, T., & Cox, J. (2016). The MaxQuant computational platform for mass spectrometry-based shotgun proteomics. *Nature Protocols, 11*(12), 2301–2319. https://doi.org/10.1038/nprot.2016.136.

Waterhouse, A., Bertoni, M., Bienert, S., Studer, G., Tauriello, G., Gumienny, R., Heer, F. T., de Beer, T. A. P., Rempfer, C., Bordoli, L., Lepore, R., & Schwede, T. (2018). SWISS-MODEL: homology modelling of protein structures and complexes. *Nucleic Acids Research, 46*(W1), W296–W303. https://doi.org/10.1093/nar/gky427.

Wu, R. B., Wu, C. L., Liu, D., Yang, X. H., Huang, J. F., Zhang, J., Liao, B., & He, H. L. (2018). Antioxidant and anti-freezing peptides from salmon collagen hydrolysate prepared by bacterial extracellular protease. *Food Chemistry, 248*, 346–352.

Xu, L., Liang, G., Shi, S., & Liao, C. (2018). SeqSVM: A sequence-based support vector machine method for identifying antioxidant proteins. *International Journal of Molecular Sciences, 19*(6), 1773. https://doi.org/10.3390/ijms19061773.

Yesiltas, B., Sørensen, A.-D.-M., García-Moreno, P. J., Anankanbil, S., Guo, Z., & Jacobsen, C. (2019). Modified phosphatidylcholine with different alkyl chain length and covalently attached caffeic acid affects the physical and oxidative stability of omega-3 delivery 70% oil-in-water emulsions. *Food Chemistry, 289*(1), 490–499. https://doi.org/10.1016/j.foodchem.2019.03.087.